Pericentrin and γ-Tubulin Form a Protein Complex and Are Organized into a Novel Lattice at the Centrosome

Jason B. Dictenberg,* Wendy Zimmerman,* Cynthia A. Sparks,‡ Aaron Young,* Charles Vidair,§ Yixian Zheng,‖ Walter Carrington,¶ Fredric S. Fay,†¶ and Stephen J. Doxsey*

*Program in Molecular Medicine and Department of Cell Biology, University of Massachusetts Medical Center, Worcester, Massachusetts 01655; ‡Worcester Foundation for Biomedical Research, Shrewsbury, Massachusetts 01545; §Department of Radiation Oncology, University of California, San Francisco, California 94143-0806; ‖Department of Biology, Carnegie Institute of Washington, Baltimore, Maryland 21210; and ¶Biomedical Imaging Group, University of Massachusetts Medical Center, Worcester, Massachusetts 01655

Abstract. Pericentrin and γ-tubulin are integral centrosome proteins that play a role in microtubule nucleation and organization. In this study, we examined the relationship between these proteins in the cytoplasm and at the centrosome. In extracts prepared from *Xenopus* eggs, the proteins were part of a large complex as demonstrated by sucrose gradient sedimentation, gel filtration and coimmunoprecipitation analysis. The pericentrin–γ-tubulin complex was distinct from the previously described γ-tubulin ring complex (γ-TuRC) as purified γ-TuRC fractions did not contain detectable pericentrin. When assembled at the centrosome, the two proteins remained in close proximity as shown by fluorescence resonance energy transfer. The three-dimensional organization of the centrosome-associated fraction of these proteins was determined using an improved immunofluorescence method. This analysis revealed a novel reticular lattice that was conserved from mammals to amphibians, and was organized independent of centrioles. The lattice changed dramatically during the cell cycle, enlarging from G1 until mitosis, then rapidly disassembling as cells exited mitosis. In cells colabeled to detect centrosomes and nucleated microtubules, lattice elements appeared to contact the minus ends of nucleated microtubules. Our results indicate that pericentrin and γ-tubulin assemble into a unique centrosome lattice that represents the higher-order organization of microtubule nucleating sites at the centrosome.

A major function of centrosomes in animal cells is to nucleate microtubules. Pericentrin and γ-tubulin are centrosome proteins that are involved in microtubule nucleation and organization, although their precise roles in these processes have not been determined (Oakley and Oakley, 1989; Archer and Solomon, 1994; Doxsey et al., 1994; Zheng et al., 1995; Merdes and Cleveland, 1997). They are both found at centrosomes and other microtubule organizing centers (MTOCs)[1] in a wide range of organisms. At the centrosome, they are localized within the centrosome matrix, which is the material that surrounds the centriole pair and nucleates microtubules (Gould and Borisy, 1977). They are also present in a soluble form in the cytoplasm of somatic cells and in *Xenopus laevis* egg extracts. Since they share common cellular sites and are both required for microtubule-associated processes, it is possible that these proteins function by interacting directly or through other proteins to coordinate microtubule nucleation in the cell.

For over one hundred years, little progress has been made in understanding the structural organization of the centrosome matrix or pericentriolar material (PCM; Wilson, 1925; Kellogg et al., 1994). The higher resolving power of EM has been of limited use in identifying the structure of the matrix, as it appears as a complicated tangle of fibers and granular material with proteins that nonspecifically associate (Kellogg et al., 1994). Although immunogold EM techniques have provided useful information on the localization of specific molecular components at the centrosome (Doxsey et al., 1994; Stearns and Kirschner, 1994; Moritz et al., 1995), they too are limited in their abil-

†Dr. F.S. Fay died on March 18, 1997.

Address all correspondence to Stephen J. Doxsey, Program in Molecular Medicine, University of Massachusetts Medical Center, Worcester, MA 01655. Tel.: (508) 856-1613. Fax: (508) 856-4289. E-mail: stephen.doxsey@ummed.edu

1. *Abbreviations used in this paper*: CCD, charge-coupled device; GFP, green fluorescent protein; FRET, fluorescence resonance energy transfer; γ-TuRC, γ-tubulin ring complex; MTOC, microtubule organizing center.

ity to reveal the overall three-dimensional (3D) organization of these molecules because of problems associated with loss of antigenicity and reagent penetration (Griffiths, 1993). Recently, ringlike structures with diameters similar to microtubules (25–28 nm) have been found in centrosomes of *Drosophila* (Moritz et al., 1995) and *Spisula* (Vogel et al., 1997), where they appear to contact ends of nucleated microtubules. γ-Tubulin has been localized to these rings (Moritz et al., 1995), and is also part of a soluble protein complex of similar geometry called the γ-tubulin ring complex (γ-TuRC), which is sufficient for microtubule nucleation in vitro (Zheng et al., 1995). Aside from the rings and the ill-defined fibrogranular material, little is known about the assembly and organization of the centrosome matrix.

Assembly of microtubule nucleating complexes onto centrosomes is considered to be a key event in regulating nucleating activity of cells (Kellogg et al., 1994). In mitosis, the higher level of centrosome matrix material and the increase in microtubule nucleation is believed to be required for proper assembly of the mitotic spindle (Kuriyama and Borisy, 1981; Kellogg et al., 1994). Assembly of microtubule asters in *Xenopus* egg extracts has been shown to require soluble pericentrin and γ-tubulin (Archer and Solomon, 1994; Doxsey et al., 1994; Stearns and Kirschner, 1994; Felix et al., 1994). Although it has been hypothesized that pericentrin may provide a structural scaffold for microtubule nucleating complexes at the centrosome (Doxsey et al., 1994; Merdes and Cleveland, 1997), the precise role of the protein in centrosome organization and microtubule nucleation has not been determined.

In this study, we demonstrate that pericentrin and γ-tubulin are components of a large protein complex in *Xenopus* egg extracts. When assembled at the centrosome, the proteins form a unique reticular lattice when analyzed by an improved immunofluorescence method (Carrington et al., 1995). The lattice is conserved from mammals to amphibians, it is organized independent of centrioles, and it appears to nucleate microtubules. Based on these observations, we propose that the pericentrin–γ-tubulin lattice plays a role in microtubule nucleation and organization in perhaps all animal cells.

Materials and Methods

Antibodies

A polyclonal antibody raised in rabbits against the NH_2 terminus of pericentrin (glutathione-S-transferase [GST]-pericentrin 2) (Doxsey et al., 1994) was affinity purified (M8) and used, unless otherwise stated. In addition, a rat monoclonal antibody was made against a 561–amino acid polypeptide (1,293–1,853) at the COOH terminus of pericentrin (A102). IgG from cell supernatants was purified by protein A binding (Harlow and Lane, 1988), concentrated and used at 2 μg/ml for immunofluorescence studies where indicated. A third pericentrin antibody was used to confirm immunoprecipitations of pericentrin from *Xenopus* extracts (RAT2, see below). This antibody was raised against gst-pericentrin 2 in a rat; it recognized pericentrin in *Xenopus* centrosomes both by immunofluorescence and by immunoblotting (data not shown). Several polyclonal (Stearns and Kirschner, 1994; Zheng et al., 1995) and monoclonal antibodies (Novakova et al., 1996) (T-6557; Sigma Chemical Co., St. Louis, MO) to γ-tubulin were used for immunoprecipitations, immunofluorescence, and immunoblotting as indicated. Antibodies to centrin and p50 were used as described (Salisbury, 1995; Echeveri et al., 1996). Cyclin antibodies were obtained from Santa Cruz Biotechnology (Santa Cruz, CA).

Cells and Cell Synchrony

Cell lines (CHO, COS, *Xenopus* tissue culture, and XTC) were grown as described (American Type Culture Collection, Rockville, MD) and mouse eggs were obtained as described (Doxsey et al., 1994). Highly synchronized mitotic CHO cells were released and collected at various stages of the cell cycle (Sparks et al., 1995). Cell cycle stage was determined by time after release from metaphase, DNA morphology, microtubule pattern and centrosome number and position as described (Sparks et al., 1995). In some cases, cells were released in the presence of cycloheximide (10 μg/ml; Sigma Chemical Co.).

Preparation of Cell Lysates and Xenopus Extracts

Xenopus extracts were prepared from eggs arrested in mitosis and interphase, centrifuged at high speed as described (Murray and Kirschner, 1989; Stearns and Kirschner, 1994), and used for immunoprecipitations, immunodepletions, sucrose gradients, and aster assembly reactions. Spindles and half spindles were prepared as described (Sawin and Mitchison, 1991; Walczak and Mitchison, 1996). COS cell lysates were prepared after release of cells from plates with trypsin and pelleting. Cells were washed in Hepes 100 buffer with 0.1 mM GTP and protease inhibitors (Zheng et al., 1995), and then lysed by sonication. Lysates were spun at 100,000 *g* for 30 min, and the supernatant was used for immunoprecipitations and sucrose gradients. Mitotic CHO cells were pelleted, boiled in 0.1% SDS in 50 mM Tris, pH 7.6, sonicated, and then diluted 1:20 with PBS containing 0.5% BSA. Reagents were added to lysates to achieve concentrations in radioimmunoprecipitation assay (RIPA) (Sparks et al., 1995), and immunoprecipitations were done with antibodies to pericentrin and Western blots were done with antibodies to γ-tubulin (see below).

Immunoprecipitation and Western Blotting

Antibodies to γ-tubulin, pericentrin (5 μg IgG), and preimmune IgGs (8 μg IgG) were prebound to 20 μl of packed protein A beads (GIBCO BRL, Gaithersburg, MD), and then added immediately to freshly prepared extracts. After incubation in 100 μl of *Xenopus* extract or cell lysate for 1 h at 4°C, beads were washed in Hepes 100 buffer with 1 mM GTP and protease inhibitors (Zheng et al., 1995) with or without 0.1% Triton X-100 or 250 mM NaCl (Sigma Chemical Co.), and proteins were run on 7% gels unless otherwise stated. Controls included extracts incubated with either preimmune sera (pericentrin), rabbit IgG, or beads alone (γ-tubulin and pericentrin). γ-Tubulin preimmune sera (Zheng et al., 1995) is no longer available. No bands were observed under any of these conditions. Proteins were electrophoretically transferred to immobilon (Millipore Corp., Bedford, MA) and immunoblotted (Harlow and Lane, 1988). When possible, blotting was performed with antibodies from another species so IgGs used for IPs were not detected by secondary antibodies. Immunoblotting of γ-tubulin was performed with one of two mouse monoclonal antibodies (Tu-31 or T-6557; Sigma Chemical Co.) or polyclonal antibody (Zheng, 1995); blotting of pericentrin was done with M8. For immunodepletions, 7.5 μg of γ-tubulin IgG was used per 50 μl of extract, which was 30% more than that required to remove all detectable γ-tubulin from extracts as judged by consecutive immunoprecipitations (IPs) with 5 μg of antibody and Western blot. SDS-PAGE and immunoblotting were performed essentially as described (Harlow and Lane, 1988). The bands (~100 kD) seen in pericentrin immunoprecipitations probed with pericentrin antibodies (see Fig. 3 *B*) were probably nonspecifically associated as they were never seen in isolated centrosome fractions (see Fig. 3 *A*), they were not consistently observed in extracts, they did not co-migrate with the γ-tubulin or pericentrin fractions in sucrose gradients (data not shown), and they were not seen with the RAT2 antibody (data not shown).

Sucrose Gradients, Gel Filtration, and Stoichiometry

Sucrose gradient sedimentation (continuous 10–40%) was performed on crude and high speed supernatants of *Xenopus* extracts (100 μl), COS cell lysates (150 μl), or reticulocyte lysates containing in vitro–translated, [^{35}S]methionine-labeled, full-length mouse pericentrin (20 μl, TNT kit; Promega Corp., Madison, WI) (Doxsey et al., 1994) essentially as described (Stearns and Kirschner, 1994). In some cases Triton X-100 (0.1%) or NaCl (250 mM) was included in the gradients and the extracts. Sucrose gradient fractions were exposed to SDS-PAGE and immunoblotted with either M8 or Tu-31. Similar results were obtained by probing with M8, stripping the same blot (Harlow and Lane, 1988) and reprobing with Tu-31.

For gel filtration experiments, crude *Xenopus* extracts (1–10 mg, see above) were prepared and kept on ice for various times (30–120 min). Extracts were diluted (1:2 to 1:4) into Hepes 100 with 10% glycerol, protease inhibitors, and GTP (final 0.1 mM) and passed through a prewetted 0.45 μm Millex-GV low protein binding filter (Millipore Corp.). Filtered extract was exposed to fast pressure liquid chromatography using a Superose-6 gel filtration column (Pharmacia Biotechnology Inc., Piscataway, NJ) equilibrated in Hepes 100 buffer with 10% glycerol at 0.3 ml/min. Fractions (0.5 ml) were collected, protein was precipitated with trichloroacetic acid, and then samples were processed for immunoblotting as above.

Standards for sucrose gradients and gel filtration analyses were run at the same time and under the same conditions as experimental samples. Standards included thyroglobulin (19.4S, 8.4 nm, Stokes radius), apoferritin (6.7 nm, Stokes radius), catalase (11.4S), alcohol dehydrogenase (3.58S) (DeHaen, 1987; Jacobson et al., 1996) and other conventional lower molecular mass standards (Sigma Chemical Co.). Values for Stokes radius were determined by gel filtration as described (Siegel and Monty, 1966), and sedimentation coefficients were estimated by sucrose density sedimentation (Martin and Ames, 1960) using published tables of sucrose density and viscosity (deDuve et al., 1959). Our gradients deviate from linear so only approximate ranges for S values at high sucrose concentration were determined. The estimated S values and Stokes radii were used to estimate the molecular mass of the protein complexes as described (Siegel and Monty, 1966) assuming a partial specific volume of 0.74 ml/g (DeHaen, 1987).

The ratio of pericentrin to γ-tubulin in the holocomplex and the number of molecules in extracts was estimated by quantitative Western blot using bacterially expressed proteins as standards (Doxsey et al., 1994; Stearns and Kirschner, 1994) (γ-tubulin clone was a gift from B. Oakley, Ohio State University, Columbus, OH). Pericentrin was not detectable in *Xenopus* extracts without enrichment, so sucrose gradient fractions were used for quantitation, and both proteins were quantified within the same experiment. Signals in the linear response range were quantified using a Fluor/S Multiimager (Bio-Rad Laboratories, Hercules, CA). Values represent averages from five experiments in which individual values were obtained in triplicate. From these results, we determined that pericentrin represented ~0.001% of the total protein in extracts and values obtained for γ-tubulin were in agreement with those previously published (0.01% of total protein; Stearns and Kirschner, 1994). The molar ratio of pericentrin to γ-tubulin was estimated to be ~1:30 ($n = 4$).

Preparation of Cells and Cell Fractions for Imaging

Unless otherwise indicated, cells were permeabilized in 0.5% Triton X-100 in 80 mM Pipes, 1 mM $MgCl_2$, 5 mM EGTA, pH 6.8, fixed in −20°C MeOH, and then processed for immunofluorescence as described previously (Doxsey et al., 1994). Several other methods were used to confirm the lattice structure including: 1 or 2% glutaraldehyde in PBS ± 5 mM Ca^{2+} followed by MeOH after fixation, 4% formaldehyde in PBS, 4% formaldehyde with 0.05% glutaraldehyde in PBS, quick freeze at liquid helium temperature (4 degrees kelvin), followed by freeze substitution in acetone alone (Nicolas and Bassot, 1993), in acetone with 1.5% glutaraldehyde, and in MeOH with 1.5% glutaraldehyde. No differences were observed in lattice structure under any of these conditions or if cells were permeabilized before fixation.

Centrosome images in Fig. 4, *C–F* were obtained from an unfixed CHO cell permeabilized for 60 s and incubated for 7 min with M8 (20 μg/ml). After washing (10 changes in 1 min), cells were incubated in cy3 donkey anti–rabbit IgG (cyDAR; Jackson Immunoresearch Laboratories, Inc., West Grove, PA) at 25 μg/ml for 5 min, washed 10 times in 1 min, mounted unfixed in Vectashield (Vector Labs, Inc., Burlingame, CA), and then imaged immediately.

Mouse oocytes arrested in metaphase of meiosis II were affixed to polylysine-coated coverslips, fixed in −20°C MeOH and processed to visualize pericentrin, microtubules, and DNA as described (Doxsey et al., 1994). *Xenopus* asters and spindles were labeled with antibodies to α-tubulin, pericentrin (M8, or γ-tubulin, Tu-31), and 4,6-diamidino-2-phenylindole (DAPI) as described (Doxsey et al., 1994). Centrosomes were isolated as described (Blomberg and Doxsey, 1998), and then immunostained for pericentrin.

Expression of Green Fluorescent Protein–Pericentrin

The S65T mutant of Green Fluorescent Protein (GFP) (Heim et al., 1995) was cloned into Xho and EcoRI sites of the plasmid pcDNA3 (InVitrogen, San Diego, CA). EcoRI sites were engineered onto the ends of amino acids 766–1,343 of pericentrin clone λpc1.1 (Doxsey et al., 1994) using PCR primers p2595 (5′-GCGAATTCATGCTGAAACGCCAACATGCTGAAGAGC-3′) and p4322 (5′-GCGAATTCCTCGAGGCGCTTAATTTC-3′). The fragment was cloned into the pcDNA3 vector and the sequence was found to be identical to that in the original clone. The construct was transfected into COS cells as described (2 μg, Lipofectamine; GIBCO BRL). Centrosome localization of the chimeric protein was shown by colocalization of GFP fluorescence with endogenous pericentrin labeled by immunofluorescence with M8. Centrosomes were imaged live in a 37°C, CO_2-perfused chamber 72 h after transfection; identical results were obtained with the full-length pericentrin. Incorporation of GFP–pericentrin into the centrosome lattice confirmed the structure seen by immunofluorescence and controlled for potential artifacts introduced during specimen preparation such as fixation, permeabilization, and antibody binding. On average, the lattice elements were slightly thinner (76 ± 9 nm) than those imaged after indirect immunofluorescence (95 ± 11 nm), suggesting that antibodies (15 nm in length) used for indirect immunofluorescence increased lattice dimensions.

Microtubule Regrowth

For imaging microtubule–lattice contacts, CHO cells were prepared essentially as described (Brown et al., 1996). Briefly, cells were treated with nocodazole (10 μg/ml) for 1.5 h at 37°C, washed rapidly five times in PBS at 37°C and incubated for various times at 37°C in medium. Cells were fixed and stained for α-tubulin and pericentrin as for centrosomes (above) and those demonstrating clear microtubule nucleation at the earliest time point (usually 1–2 min) were used for analysis (below). Microtubule nucleation times were kept to a minimum to minimize the possible release of microtubules from nucleating sites (Mogensen et al., 1997).

Image Acquisition and Deconvolution

Images were recorded on a cooled CCD camera (Photometric, Tucson, AZ) using a Nikon inverted microscope and a 100× PlanApo objective with a 1.4 numerical aperture (N.A.). Images were taken at 100-nm intervals through focus (in z plane) with 56 nm per pixel (x, y), and restored to subvoxels of 28 × 28 × 50 nm as described (Carrington et al., 1995). Images in Fig. 6 were taken with a 60× PlanApo, N.A. = 1.4. Fluorescent beads (189 nm) were imaged under the same optical conditions as the cell, and the microscope point spread function (PSF) was calculated on a subpixel grid. The dye density was then estimated by the non-negative function, *f*, that minimizes

$$\|g - PSF \times f\|^2 + \alpha \iiint |f|^p,$$

where *g* is the measured cell image. Resolution of images was improved over previous studies by using values of $P < 2$. Images were reconstructed according to the algorithm with the following range of parameters: $\alpha = 10^{-7}$–10^{-12}, $P = 1.08$–2 with 1,000–1,500 iterations. The images were gradient shaded, displayed as three-dimensional projections, and in some cases pseudocolored.

Other structures imaged by this technique included a mitochondrial inner membrane protein (MCA-151A; Harlan Sprague Dawley Inc., Indianapolis, IN), a lysosomal membrane protein (provided by S. Green, University of Virginia, Charlottesville, VA), an *Escherichia coli* outer membrane protein (PLA protease; J. Goguen, University of Massachusetts Medical Center, [UMMC], Worcester, MA), and DNA of somatic cells and bacteria. DNA had the characteristic pattern described recently using a similar technique (Urata et al., 1995). As described in the text, centrioles imaged by this technique consistently had barrel diameters of 230 ± 11 nm ($n = 23$), similar to that seen by electron microscopy (~200 nm). Centriole length was more variable (350–500 nm) possibly because of impeded access of antibody at centriole ends enveloped by the lattice. In fact, the length of basal bodies (centrioles that lack lattice material) in tracheal epithelium (450–550 nm, $n = 14$; data not shown), were closer to the length expected from electron microscopy (500 nm).

Quantitation of Fluorescence Signals from Centrosomes

To quantify centrosome protein levels through the cell cycle (see Fig. 8), CHO cells were fixed in −20°C MeOH and stained for pericentrin (M8) and γ-tubulin (Tu-30) together or separately. Two-dimensional digital images were captured on a CCD camera and processed on a Silicon Graphics workstation (Mountain View, CA). A square measuring 71 × 71 pixels

(~4 × 4-μm box) was centered on the centrosome and the mean intensity per pixel was determined. Background values recorded by the same method in another area of the cytoplasm and those used to correct for camera noise were subtracted and accounted for <5% of experimental values. Similar results were obtained in five separate experiments and when secondary antibodies were switched. Values for each experiment were obtained from cells on a single coverslip. Similar results were obtained with COS cells. Each time point represents an average of 15–35 values. Similar results were obtained using an Adherent Cell Analysis System (ACAS 570; Meridian Instruments, Ann Arbor, MI). To determine the relative amount of pericentrin at the centrosome and in the cytoplasm, nonpermeabilized cells were used, and the total cellular and centrosomal levels were determined as above. Cytoplasmic fluorescence was calculated by subtracting centrosomal from total cellular fluorescence. The distribution of the pericentrin fluorescence changed in mitosis, although the total cellular fluorescence remained the same.

Coincidence of Fluorescence Signals and Fluorescence Resonance Energy Transfer

The data analysis and visualization environment (DAVE) (Lifschitz et al., 1994) was used to visualize images in three dimensions, to superimpose them, and to determine the extent to which they coincided. Staining coincidence was determined by imaging centrosomes within a 2-μm^3 area that included all detectable fluorescence in both wavelengths; smaller volume measurements gave similar values. To ensure proper alignment, fiducial beads were used (Carrington et al., 1995). Colocalization was expressed as the number of 28-nm voxels (volume pixels) occupied by two signals over all voxels occupied by the pericentrin signal all non-zero voxels were included in the analysis. Colocalization statistics were unaffected by any visual aids used to modify images. Microtubule–lattice contacts were determined in a similar fashion by statistical analysis of coincident signals between microtubule ends and lattice elements. The percentage of microtubule ends contacting the lattice was similar when either pericentrin or γ-tubulin was used to stain the lattice.

Fluorescence resonance energy transfer (FRET) is a distance-dependent interaction between two fluorophores in their excited states where the excitation of the donor molecule (FITC) is transferred to an acceptor molecule (TRITC) without the emission of a photon. If FRET occurs, it can be monitored by the quench of the donor and the sensitized emission of the acceptor (Stryer, 1978; Wu and Brand, 1994). We created a FRET imaging system and calibrated it by adapting the methods of Ludwig et al. (1992). The two greatest obstacles to accurate, semi-quantitative FRET measurement using this system are filter bleedthrough and photobleaching. To measure sensitized emission, we created a "transfer" (FITC to TRITC) filter setup—480-nm excitation, but emission at >570 nm. Using this filter configuration, FITC excitation results in some non-FRET donor bleedthrough to the 570-nm emission (due to spectral emission overlap) as well as causing some direct (non-FRET) excitation of acceptor (due to spectral excitation overlap). These values were empirically measured with pure dye samples (conjugated to IgG) and later subtracted to correct the data (see below). In addition, we normalized the three-dimensional data sets to the original unbleached intensities by initially imaging single planes of each channel.

CHO cells were prepared for immunofluorescence (above) using pericentrin (M8 antibody) as the donor and the second antigen (γ-tubulin, centrin, or A102 antibody) as acceptor. Using a Nikon inverted epifluorescence microscope equipped with a CCD camera we recorded single-plane images of each contributing antigen in the transfer channel, and then three-dimensional sets were captured with identical exposure times. Images were prepared for restoration (above) except that plane normalization was set to the single-plane values recorded before three-dimensional sets. After restoration and alignment, the empirically calculated spectral overlap (mean ± 3 standard deviations) contributed by FITC and TRITC were subtracted from the transfer channel on a voxel-by-voxel basis, accounting for >99% of the total possible bleedthrough. The resulting image pairs for each set of antigens were subjected to two analyses to detect genuine FRET: (*1*) all nonzero voxels of the corrected sensitized emission (transfer channel) were displayed as a three-dimensional projection with the same scale for linear comparison of intensities and distribution, and second, the ratio of the sensitized emission to the donor emission was calculated (transfer/ FITC) within identical subregions of the corrected images. This ratio analysis relies on both donor quench and sensitized emission and is therefore very sensitive to FRET (Adams, 1991; Ludwig, 1992; Miyawaki, 1997). The means (n = 10–12) were determined within a 140-nm square throughout several regions of the image chosen randomly, and the mean ± SD were calculated for each antigen pair (n = 3).

Results

Pericentrin and γ-Tubulin Are Part of a Protein Complex in Xenopus Extracts

Xenopus eggs are an excellent source of centrosome components as each stockpiles material sufficient to assemble ≤2,000 centrosomes (Gard et al., 1990). These components assemble into centrosomes upon fertilization and throughout the early divisions of the embryo. We characterized the state of pericentrin in *Xenopus* egg extracts by sucrose gradient sedimentation, gel filtration analysis, and immunoprecipitation experiments. We used antibodies previously generated against a mouse recombinant protein that recognized *Xenopus* centrosomes by immunofluorescence (Doxsey et al., 1994) and reacted with a single protein of ~210 kD in *Xenopus* centrosome fractions, similar in molecular mass to mouse pericentrin.

In freshly prepared extracts subjected to sucrose gradient centrifugation, pericentrin migrated in the high density fractions, suggesting that it was in the form of a large protein complex (Fig. 1 *B*). This was in contrast to the protein produced by in vitro translation of pericentrin mRNA, which sedimented much more slowly (Fig. 1 *A*). The sedimentation properties of pericentrin were roughly similar to those previously observed for γ-tubulin (Stearns and Kirschner, 1994; Zheng et al. 1995), suggesting that the proteins may be part of the same complex. When analyzed together in the same experiment, the proteins were found to comigrate in sucrose gradients (Fig. 1, *B* and *C*). Moreover, when extracts were subjected to gel filtration analysis, both proteins co-eluted in the same fractions (Fig. 2 *A*). These results indicate that pericentrin and γ-tubulin are either part of the same complex or components of distinct complexes with similar biochemical properties.

To distinguish between these possibilities, we performed a series of immunoprecipitation experiments (Fig. 3). When γ-tubulin was immunoprecipitated from extracts, pericentrin was detected by immunoblotting (Fig. 3 *C*); conversely, when pericentrin was immunoprecipitated from extracts, γ-tubulin was detected on immunoblots (Fig. 3 *E*). Similar results were obtained when immunoprecipitations were performed with different antibodies to pericentrin and γ-tubulin and when mammalian cell extracts were used (data not shown). In contrast, neither protein was detected when preimmune IgGs or immunobeads were used (Fig. 3, *F* and *G*). When γ-tubulin was exhaustively immunodepleted from extracts, the majority (85–95%) of pericentrin was depleted as well. This was most clearly demonstrated when immunodepleted extract was analyzed on sucrose gradients (Fig. 1, *D* and *E*) and compared with starting material (Fig. 1, *B* and *C*). Taken together, the results from three independent biochemical methods demonstrate that most, if not all, of the pericentrin and γ-tubulin in *Xenopus* extracts is in the form of a large complex.

Pericentrin Is Not Part of the γ-TuRC

The association of pericentrin with a large protein com-

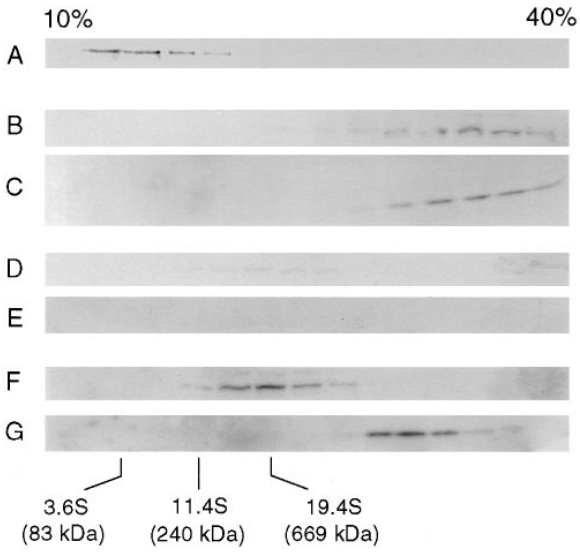

Figure 1. Pericentrin and γ-tubulin cosediment in sucrose gradients. (*A*) In vitro–translated, [^{35}S]methionine-labeled mouse pericentrin was sedimented in sucrose gradients (10–40%) and exposed to SDS-PAGE as described in Materials and Methods. (*A* and *B*) *Xenopus* extracts were sedimented in sucrose gradients and immunoblotted using antibodies to pericentrin (*B*) or γ-tubulin (*C*). Parallel sample of the same extract immunodepleted of γ-tubulin (*D* and *E*) or treated with 0.1% Triton X-100 (*F* and *G*) before gradient centrifugation. Pericentrin immunoblots (*B*, *D*, and *F*); γ-tubulin immunoblots (*C*, *E*, and *G*). Molecular weight standards are for all panels.

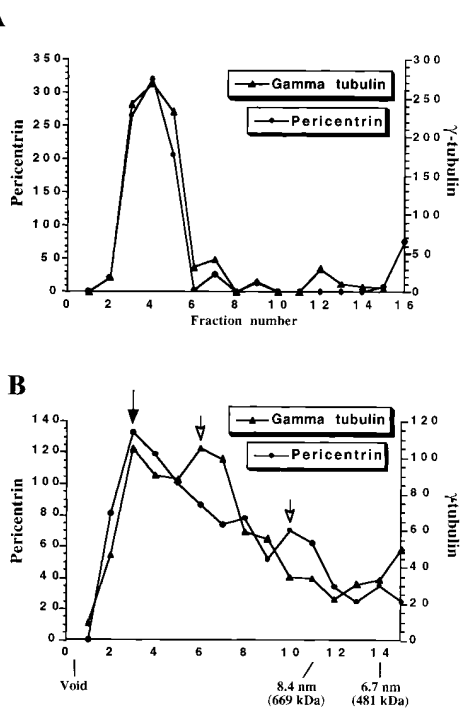

Figure 2. Pericentrin and γ-tubulin cofractionate by gel filtration. *Xenopus* extracts were fractionated by gel filtration using a Superose-6 column. Proteins were precipitated from fractions with trichloroacetic acid, immunoblotted using antibodies to pericentrin or γ-tubulin, and then resulting bands were quantified (see Materials and Methods for details). Under optimal conditions, the majority of γ-tubulin and pericentrin eluted together in fractions *3–5*, suggesting that they were part of a large complex (*A* and *B*, *closed arrow*). A variable portion of pericentrin eluted at fractions *5–7* and γ-tubulin at *9–11* (*B*, *open arrows*) when extracts were incubated for extended periods on ice (1 h). Y axes represent units of band intensity from Western blots.

plex containing γ-tubulin suggested that it may be part of the γ-TuRC. To our surprise, pericentrin was not detectable in purified γ-TuRC preparations (Zheng et al., 1995), even when the γ-tubulin signal was fivefold greater than that detected in immunoprecipitations (Fig. 3, *H* and *I*). A clue to this apparent discrepancy came when immunoprecipitates were washed with nonionic detergent or 250 mM salt. Under these conditions, pericentrin was no longer detected in γ-tubulin immunoprecipitations (data not shown). Furthermore, the proteins no longer comigrated on sucrose gradients in the presence of detergent, but sedimented as distinct subcomplexes in fractions of lower density (Fig. 1, *F* and *G*). γ-Tubulin shifted only slightly, whereas pericentrin shifted several fractions; the slight shift in γ-tubulin may have gone undetected in previous studies (Stearns and Kirschner, 1994). In gel filtration experiments, disruptive conditions (e.g., extended periods on ice) also yielded two separate subcomplexes (Fig. 2 *B*, *open arrows*). The sensitivity of the large complex to these and other treatments was decreased in the presence of glycerol and was variable between extract preparations.

Results from these biochemical analyses were used to estimate the molecular mass of the complex. From the sucrose gradients, we estimated the sedimentation coefficient of the complex to be 38–48S. From gel filtration experiments, we estimated the Stokes radius of this large complex as ~15–16.5 nm. On the basis of the sedimentation coefficient and the Stokes radius, we calculated the relative molecular mass of the complex to be 2.5–3.5 MD as described (Siegel and Monty, 1966) using a partial specific volume of 0.74 (DeHaen, 1987). The stoichiometry of pericentrin and γ-tubulin in extracts was determined by quantitative analysis of immunoblots using recombinant proteins as standards (see Materials and Methods; Doxsey et al., 1994; Stearns and Kirschner, 1994). By this analysis, we estimated that pericentrin and γ-tubulin represented 0.001 and 0.01% of the total protein in extracts, respectively; the estimate of γ-tubulin in extracts was in agreement with previous studies (Stearns and Kirschner, 1994). The stoichiometry of the proteins was calculated to be one pericentrin molecule for every ~30 γ-tubulin molecules. Based on the stoichiometry of pericentrin and γ-tubulin and the relative molecular mass of the complex containing both proteins, we estimate that there are two γ-tubulin subcomplexes and one pericentrin subcomplex complex in each large co-complex (see Discussion).

Pericentrin Defines a Novel Lattice at the Centrosome

Identification of a soluble complex containing pericentrin and γ-tubulin suggested that these proteins may also be in close proximity at the centrosome. To address this, we examined the distribution of the proteins at the centrosome using an advanced mathematical algorithm for deconvolu-

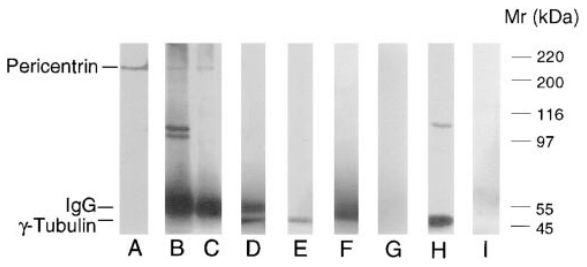

Figure 3. Pericentrin coimmunoprecipitates with γ-tubulin but is not part of the isolated γ-TuRC. Various cellular fractions were exposed to SDS-PAGE and immunoblotted with pericentrin or γ-tubulin antibodies. (*A*) Centrosome fractions prepared from *Xenopus* tissue culture cells as described (Blomberg and Doxsey, 1998) and probed with pericentrin antibodies. Pericentrin (*B*) or γ-tubulin (*C*) immunoprecipitated from freshly prepared *Xenopus* extracts and blotted with pericentrin antibodies. γ-Tubulin (*D*) or pericentrin (*E*) immunoprecipitated from freshly prepared *Xenopus* extracts and blotted with γ-tubulin antibodies. Precipitations performed with pericentrin preimmune sera and blotted with pericentrin antibodies (*F*) or with no antibody (immunobeads alone) and blotted with γ-tubulin antibody (*G*). Purified γ-TuRC fractions immunoblotted with antibodies to γ-tubulin (*H*) or pericentrin (*I*).

tion of immunofluorescence images that provides at least fourfold greater resolution than conventional imaging methods (theoretically ~70 nm) (Carrington et al., 1995). For this analysis, optical sections of centrosomes were taken every 100 nm through focus, captured on a cooled CCD camera, and then the resulting images were restored by deconvolution using the algorithm.

We initially examined the organization of pericentrin at the centrosome. By conventional imaging methods, the immunofluorescence signal for pericentrin appeared as a simple focus of material (Fig. 4, *B* and *C*) at the center of microtubule asters (Fig. 4 *A*). More detail was provided using previously developed deconvolution software based on exhaustive photon reassignment (Fig. 4 *D*; Scanalytics, Billerica, MA). When the image was restored using the advanced algorithm, a striking, highly organized reticular network was revealed (Fig. 4, *E* and *F*, stereo pair). This lattice-like structure was composed of a variable number of interconnected rings (273 ± 43-nm diam) with linear projections radiating from its periphery. Elements of the lattice were ~100 nm in width (γ-TuRC diameter is 25–28 nm, for comparison) and they sometimes formed angles of 120 degrees (e.g., Fig. 4 *E*, *bottom left*). The lattice was often surrounded by smaller unconnected aggregates of pericentrin-staining material (e.g., Fig. 4, *E* and *F*), previously shown to be pericentriolar satellites (Doxsey et al., 1994). These structures were confined to the region occupied by the centrosome (0.7–2.3-μm diam) and no other significant pericentrin-staining material was observed in the cytoplasm. Centrioles (Fig. 4, *J* and *K*) were located at the center of the pericentrin lattice (Fig. 4, *G–I*) in discrete lattice-free areas (Fig. 4 *I*) with dimensions roughly similar to those of the centriole barrels. Although not completely resolved, centrioles retained the general structure and dimensions observed by electron microscopy (~200 × 500 nm), demonstrating the high resolving power of the deconvolution method. Taken together, this analysis demonstrates that pericentrin forms a novel lattice structure that surrounds the centrioles of mammalian centrosomes.

To verify the unique structure defined by pericentrin staining, we analyzed centrosomes under a number of different conditions. The structural details were preserved under a wide range of fixation methods (e.g., quick freeze/freeze substitution), in the absence of fixation (Fig. 4, *E* and *F*) and after centrosome isolation and centrifugation onto coverslips (Fig. 4, *G–K*) (Blomberg and Doxsey, 1998). An indistinguishable structure was observed when a protein chimera of pericentrin and GFP was used to label centrosomes in living cells and imaged directly without antibody incubations (Fig. 4, *L–O*) (Prasher et al., 1992; Young et al., 1998).

We next examined the organization of pericentrin in centrosomes of other species and in morphologically different structures that function as MTOCs. A similar network of pericentrin staining was observed in centrosomes of cultured *Xenopus* cells, at the poles of *Xenopus* mitotic spindles assembled in vitro (Fig. 5, *A* and *B*), and in the elongated acentriolar poles of meiotic spindles in mouse oocytes (Fig. 5, *C* and *D*). The conserved organization of pericentrin in centrosomes of divergent organisms and in different types of MTOCs suggests that it may play an important role in centrosome function. Insight into the functional significance of the pericentrin lattice was initially provided when we examined the organization of γ-tubulin, the protein implicated in microtubule nucleation (Oakley and Oakley, 1989; Zheng et al., 1995).

Pericentrin and γ-Tubulin Are in Close Proximity in the Lattice

We examined the three-dimensional organization of γ-tubulin and its relationship to the pericentrin lattice using double-label immunofluorescence methods. Images restored at high resolution showed that the staining pattern of γ-tubulin was strikingly similar to pericentrin in centrosomes of somatic cells examined in situ (Fig. 6, *A* and *B*). Quantitative analysis of restored and aligned images using three-dimensional image analysis software (Lifschitz et al., 1994) revealed that the distribution of the pericentrin and γ-tubulin signals was nearly identical (Fig. 6 *E*). For comparison, the degree of signal overlap (Fig. 6 *E*, bar *3*) was similar to that observed when a single pericentrin antibody was detected with two different fluorophore-conjugated secondary antibodies, or when monoclonal and polyclonal pericentrin antibodies were detected with different secondary antibodies (Fig. 6 *E*, bars *1* and *2*). In contrast, other proteins that localize to the centrosome such as dynactin (Fig. 6, *C* and *E*, bar *5*; Echeveri et al., 1996) and centrin (Fig. 6 *E*, bar *4*; Salisbury, 1995) did not colocalize significantly with pericentrin, demonstrating the unique distribution of γ-tubulin and pericentrin at the centrosome.

The proximity of pericentrin and γ-tubulin at the centrosome was more directly measured using FRET, a method that has become a powerful approach for studying protein–protein interactions (Adams et al., 1991; Miyawaki et al., 1997). In cells colabeled for pericentrin (fluorescein) and γ-tubulin (rhodamine), fluorescein excitation (donor) resulted in strong, sensitized emission from rhodamine (acceptor), demonstrating energy transfer between the

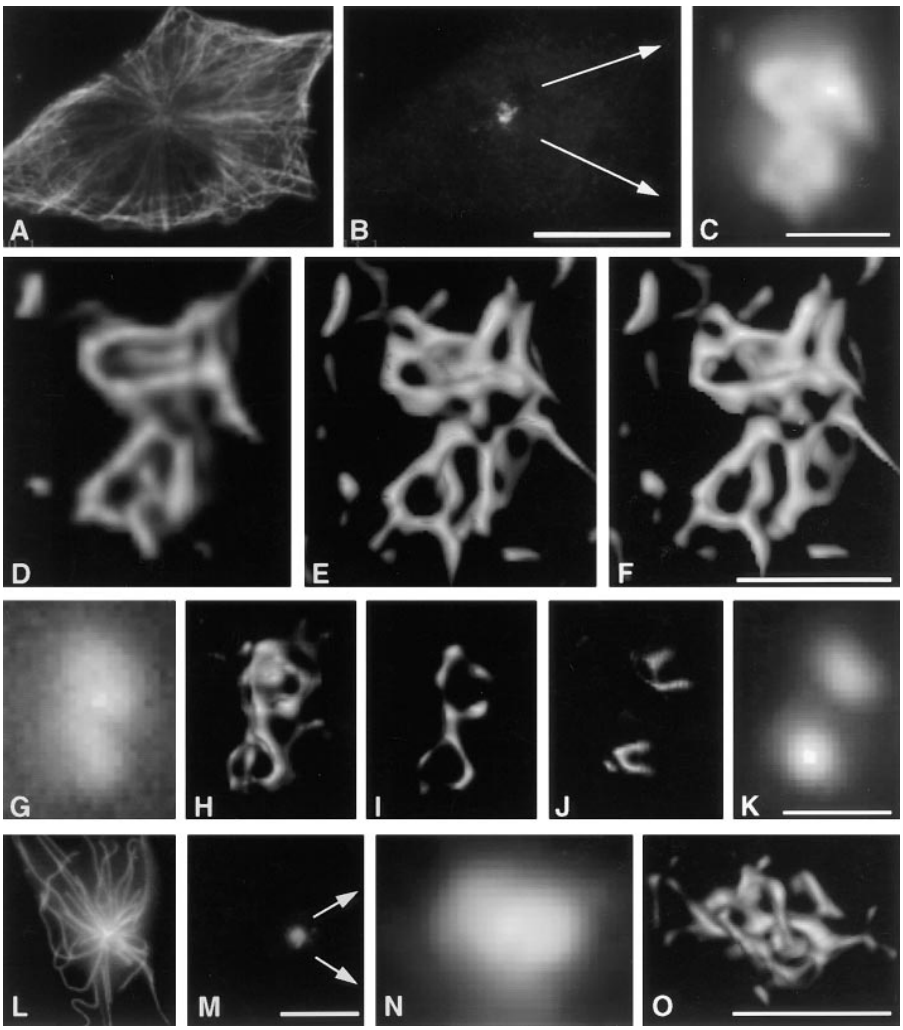

Figure 4. Pericentrin forms a novel lattice at the centrosome. Microtubule aster and centrosome from a CHO cell stained with antibodies to α-tubulin (*A*) and pericentrin (*B*) and imaged by conventional immunofluorescence methods. (*C*) High magnification of unfixed CHO cell centrosome imaged as in (*B*). (*D*) Image of same centrosome shown in (*C*) using commercially-available deconvolution software (Scanalytics). (*E* and *F*) High resolution stereo images of same centrosome in (*C*) restored by the algorithm of Carrington (1995) (*D*, +6 degrees; *E*, −6 degrees). (*G–K*) Centrosome isolated from a CHO cell and labeled with antibodies to pericentrin to visualize lattice (*G–I*) and α-tubulin to visualize centrioles (*J* and *K*). Before restoration, pericentrin (*G*) and α-tubulin (*K*). After restoration, pericentrin staining showing entire three-dimensional data set (*H*) or five central planes (*I*) and α-tubulin staining showing three central planes (*J*). The two areas devoid of pericentrin staining (*I*) represent positions occupied by centrioles (*J*). (*L–O*) GFP–pericentrin expressed in COS cells (*M*) localized to the center of a microtubule aster detected by α-tubulin immunofluorescence staining (*L*). GFP-pericentrin before (*N*) and after (*O*) image restoration. Bars: (*B*) 10 μm for *A* and *B*; (*C*) 1 μm; (*F*) 1 μm for *D–F*; (*K*) 1 μm for *G–K*; (*M*) 10 μm for *L* and *M*; (*O*), 1 μm for *N* and *O*.

proteins (Fig. 7). Restoration of the sensitized emission signal at high resolution revealed a lattice remarkably similar to that generated by the fluorescein donor signal (Fig. 7, compare *A* with *B*). To our knowledge, the acquisition of high resolution immunofluorescence images from signals generated by energy transfer is a unique and powerful application of FRET. Little energy transfer was observed when pericentrin antibodies were used in combination with centrin antibodies as shown by the low intensity of the sensitized emission, the reduced structure generated by image restoration (Fig. 7, compare *C* with *D*) and the comparatively low FRET ratio (Fig. 7 *E*, bar *3*). The FRET ratio (sensitized emission/donor emission) is another measure of energy transfer and is highest when there is strong sensitized emission and quenching of the donor (Ludwig, 1992; Wu and Brand, 1994; Miyawaki et al., 1997). The FRET ratio obtained with antibodies to pericentrin and γ-tubulin (Fig. 7 *E*, bar *2*) was similar to that obtained when two pericentrin antibodies were used (Fig. 7 *E*, bar *1*), suggesting that the proteins were in close proximity at the centrosome. Calculations based on the use of two primary–secondary antibody complexes (maximal extended length ~68 nm), and the distance at which FRET drops to <1% in this system (12 nm), suggest that the two proteins are not >80-nm apart. The proteins are likely to be much closer considering the strength of FRET and the nearly identical structure generated by the sensitized emission. The close proximity of the proteins is consistent with the idea that they remain in a complex (Figs. 1–3) after assembly at the centrosome.

Progressive Assembly and Catastrophic Disassembly of Pericentrin and γ-Tubulin during the Somatic Cell Cycle

The coexistence of pericentrin and γ-tubulin in a soluble protein complex and at the centrosome suggested a dynamic relationship between the two cellular fractions containing these proteins. As an initial test of this idea, we examined changes in the centrosome-associated fractions of the proteins in CHO cells at various cell cycle stages by quantifying immunofluorescence signals. In contrast to previous models suggesting a rapid accumulation of centrosome components shortly before metaphase (Kuriyama and Borisy, 1981), we observed a progressive increase in the centrosome-associated fraction of both proteins from basal levels in G1, to maximal levels at metaphase (Fig. 8 *A*). The total centrosomal fluorescence per cell (Fig. 8 *A*, *bottom*) increased five- to sevenfold over this time period. The kinetics of protein accumulation at the centrosome

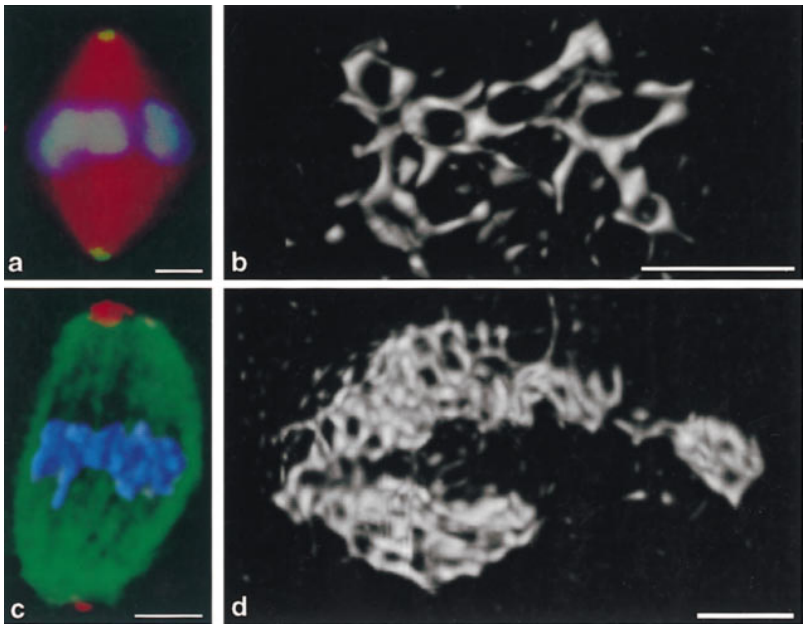

Figure 5. The lattice is a conserved feature of centrosomes and other MTOCs. (*A* and *B*) *Xenopus* spindle assembled in vitro. (*A*) Spindle labeled for pericentrin (*green*), α-tubulin (*red*), and DNA (*blue*), imaged by conventional methods and superimposed. (*B*) Restored image of centrosome at upper pole of spindle in *A*. (*C* and *D*) Acentriolar mouse meiotic spindle arrested in metaphase II. (*C*) Spindle labeled for α-tubulin (*green*), pericentrin (*red*), and DNA (*blue*) prepared as in *A*. (*D*) Restored image of spindle pole at top of image in (*C*). Note difference in magnification between *B* and *D*. Bars: (*A* and *C*) 5 μm; (*B* and *D*) 1 μm.

was nearly identical for pericentrin and γ-tubulin demonstrating that they were incorporated coordinately.

Whereas ~16 h were required to accumulate maximal levels of pericentrin and γ-tubulin at the centrosome, it took only 15–20 min for the centrosome-associated fluorescence signals to drop to basal levels as cells exited mitosis (Fig. 8 *A*, $M \rightarrow T$). This precipitous drop in centrosomal fluorescence of both proteins occurred with indistinguishable kinetics demonstrating, as in assembly, that they underwent coordinate disassembly from the centrosome. Both proteins redistributed quantitatively from the centrosome to the cytoplasm as shown by an increase in cytoplasmic fluorescence (pericentrin, 5.2×10^5 fluorescence units; γ-tubulin, 2.8×10^5 units) that occurred concomitant with a reciprocal decrease in centrosomal fluorescence (pericentrin, 4.9×10^5 units; γ-tubulin, 2.7×10^5 units). This protein redistribution occurred with no detectable change in the total cellular fluorescence or in the total biochemical levels of the proteins (Fig. 8 *B*, *1* and *2*). In fact, protein levels remained unchanged for several hours after mitosis and were unaffected when protein synthesis was inhibited (data not shown). In contrast, cyclin B was degraded to near completion during this time (Fig. 8 *B*, *3*). These results suggest that the bulk of pericentrin and γ-tubulin redistributes from the centrosome to the cytoplasm upon exit from mitosis and that the proteins are not significantly degraded during this time but are probably reused for subsequent rounds of centrosome assembly.

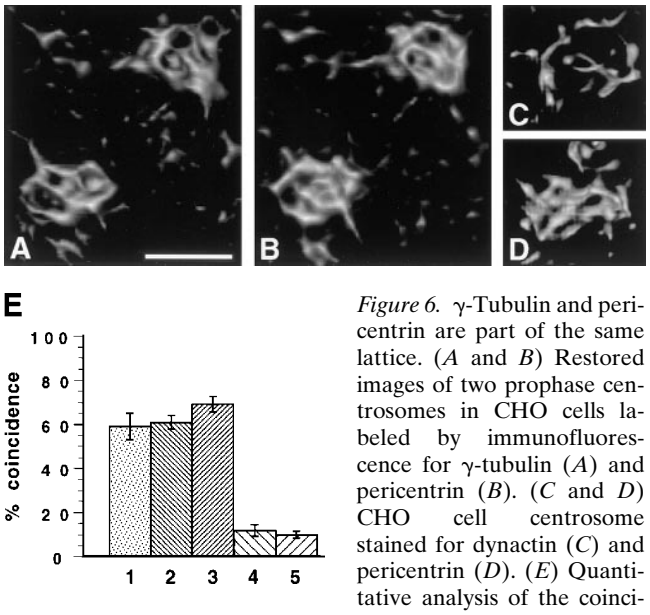

Figure 6. γ-Tubulin and pericentrin are part of the same lattice. (*A* and *B*) Restored images of two prophase centrosomes in CHO cells labeled by immunofluorescence for γ-tubulin (*A*) and pericentrin (*B*). (*C* and *D*) CHO cell centrosome stained for dynactin (*C*) and pericentrin (*D*). (*E*) Quantitative analysis of the coincidence of centrosome proteins in CHO cells using secondary antibodies tagged with different fluorophores (see Materials and Methods). Column *1*, rat anti-pericentrin/rabbit anti-pericentrin; column *2*, rabbit anti-pericentrin/mixed (fluorescein- and rhodamine-conjugated) anti–rabbit IgGs; column *3*, rat anti-pericentrin/rabbit anti–γ-tubulin; column *4*, rabbit anti-pericentrin/mouse anti-centrin; and column *5*, rat anti-pericentrin/rabbit anti-dynactin. Bar, 1 μm.

Cell Cycle Changes in the Lattice

The cell cycle changes in centrosome-associated levels of pericentrin and γ-tubulin (Fig. 8 *A*) were accompanied by dramatic changes in lattice complexity (number of rings) and overall size (Fig. 8 *C*). In G1, the lattice was smallest and least complex (Fig. 8 *C*, *left*). It enlarged progressively over a period of 16 h, reaching maximal dimensions in G2 (Fig. 8 *C*, *middle*). The lattice split in mitosis to form two metaphase structures of intermediate size and intrinsic polarity, being open at one end and rounded at the other (Fig. 8 *C*). As cells exited mitosis, the metaphase lattices rapidly disassembled (15–20 min) returning to the simple structure shown in Fig. 8 *C* (*left panel*). These data demonstrate that the dramatic cell cycle changes in the complexity of the lattice correlate closely with the levels of pericentrin and γ-tubulin at the centrosome (Fig. 8 *A*).

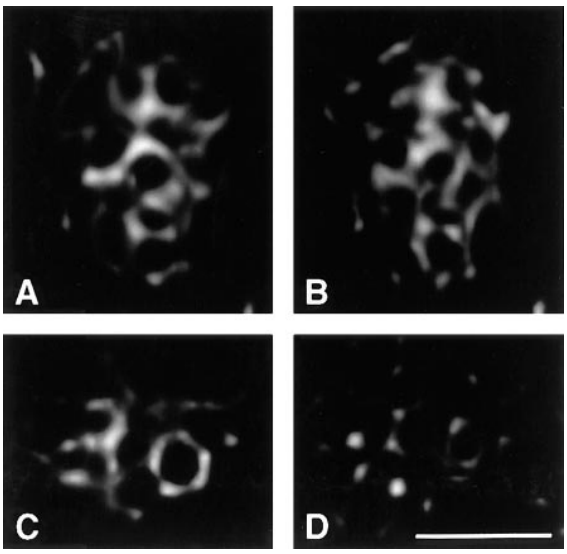

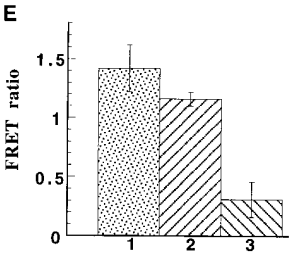

Figure 7. The proximity of γ-tubulin and pericentrin at the centrosome is sufficient to produce FRET. Centrosomes colabeled for pericentrin (*A*, fluorescein) and γ-tubulin (*B*, rhodamine), or for pericentrin (*C*, fluorescein) and centrin (*D*, rhodamine) were illuminated to excite fluorescein. Images were captured using fluorescein and rhodamine emission filters and restored as in Fig. 4. The image resulting from the transfer of energy to rhodamine-labeled antibody bound to γ-tubulin (*B*) is very similar to that generated by the donor signal (*A*). In contrast, images generated when antibodies bound to centrin serve as acceptor (*D*) represent a small subset of the pericentrin image (*C*). The FRET ratio (*E*) is expressed as the proportion of fluorescence generated by the acceptor over that generated by the donor (which is quenched after efficient transfer). The FRET ratio of pericentrin and γ-tubulin (*2*) is similar to that obtained with two pericentrin antibodies (*1*) and much greater than that of pericentrin and centrin (*3*). Bar, 1 μm.

Relationship of the Lattice and Nucleated Microtubules

Since both pericentrin and γ-tubulin have been implicated in microtubule nucleation and organization (Doxsey et al., 1994; Zheng et al., 1995) and since γ-tubulin is found at the minus ends of microtubules in the centrosome matrix (Moritz et al., 1995), we reasoned that the centrosome lattice containing these proteins may be involved in microtubule nucleation. To test this possibility, cells were treated with nocodazole to depolymerize microtubules, incubated briefly without the drug to capture early microtubule nucleation events, and then processed for immunofluorescence staining of microtubules and centrosome using the Carrington algorithm (see Materials and Methods). Microtubules were resolved as single filaments or bundled and branching arrays and nucleation sites were defined as regions of contact between the minus ends of nucleated microtubules and lattice elements (Fig. 9). Centrosomes from telophase, G1, and early S phase (Fig. 9, *S*) were used for this analysis since the microtubule–lattice contacts were clearer than in more complex centrosomes (Fig. 9, *G2*). Quantitative analysis of contact sites identified by overlapping signals (Fig. 9, *inset*, *white*) showed that most microtubule ends contacted lattice elements (79 ± 5.1%, $n = 7$ asters). These data suggest that the lattice composed of pericentrin and γ-tubulin may provide the structural basis for microtubule nucleation at the centrosome.

Discussion

The sites of microtubule nucleation in most animal cells are found primarily at centrosomes or other types of MTOCs. Here we show that pericentrin and γ-tubulin are part of a novel centrosome lattice that contacts the ends of nucleated microtubules and may provide the structural basis for microtubule nucleation. Pericentrin and γ-tubulin are also found together in a large protein complex and they assemble onto and disassemble from the lattice in a cell cycle–specific manner. These observations indicate that the pericentrin–γ-tubulin lattice may represent the higher order organization of microtubule nucleating sites at the centrosome and that assembly and disassembly of the lattice may play a role in regulating microtubule nucleation in the cell.

The Pericentrin–γ-Tubulin Complex and Centrosome Assembly

We have identified a large soluble protein complex comprised of pericentrin and γ-tubulin. Since both proteins are highly conserved through evolution (Oakley and Oakley, 1989; Doxsey et al., 1994; Zheng et al., 1995), it is possible that the complex containing these proteins is conserved in all animal cells. Disruption of the complex yields two subcomplexes (Fig. 10). One subcomplex contains γ-tubulin and may be the 25S complex previously reported (Stearns and Kirschner, 1994; Zheng et al., 1995) based on its migration in sucrose gradients. The other subcomplex contains pericentrin and has not been described previously. Little is known about the origin and composition of the pericentrin subcomplex, how it interacts with the γ-tubulin complex, and the functional consequences of this interaction. Based on the estimated masses of the complexes and the calculated stoichiometry of γ-tubulin and pericentrin (30:1), we propose that the co-complex of these proteins comprises one pericentrin complex and two γ-tubulin complexes (Fig. 10). This arrangement is consistent with both models currently proposed for microtubule nucleation. If the γ-tubulin complexes were γ-TuRCs each containing 13 γ-tubulin molecules (Zheng et al., 1995), the co-complex would contain two γ-TuRCs plus a complex with one pericentrin molecule (stoichiometry, 26:1). (More accurate modeling will require characterization of the biochemical properties of the purified γ-TuRC [Zheng et al., 1995].) If γ-tubulin complexes were pairs of protofilaments each containing ~28 γ-tubulin molecules (Erickson and Stoffler, 1996), the co-complex would contain two protofilament complexes plus a complex with two pericentrin molecules (56:2).

Based on these and other data, we propose a model for assembly of nucleating sites at the centrosome as shown in Fig. 10. The model predicts that pericentrin and γ-tubulin

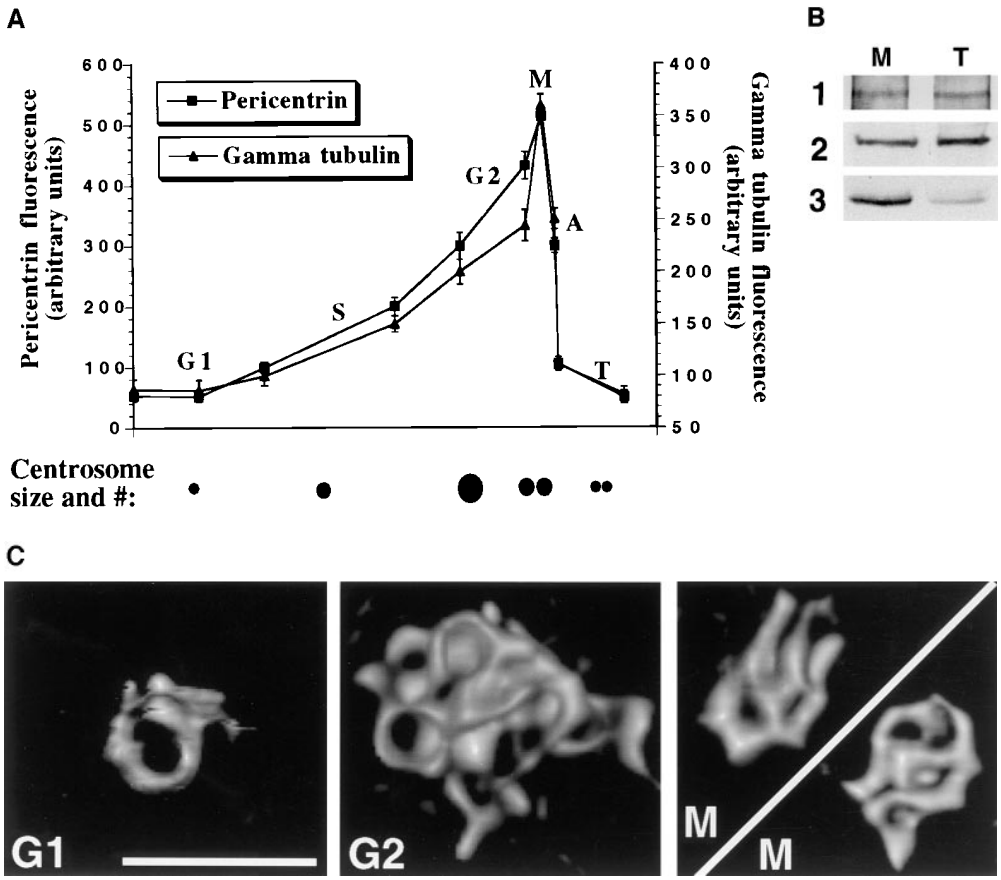

Figure 8. Dramatic cell cycle changes in the intracellular distribution of pericentrin and γ-tubulin and lattice structure. (*A*) Quantitative analysis of immunofluorescence signals from centrosome-associated pericentrin and γ-tubulin in CHO cells at various stages of the cell cycle (see Materials and Methods). Protein levels rise progressively from G1 until mitosis and then drop precipitously to basal levels. (*B*) Levels of pericentrin and γ-tubulin do not appear to change upon exit from mitosis. Lysates were prepared from metaphase cells (*M*) or from an equal number of metaphase cells induced to enter telophase (*T*; see Materials and Methods). Pericentrin was immunoprecipitated from lysates and immunoblotted with pericentrin antibodies as described in Fig. 3 (*panel 1*). Other lysates were used for immunoblotting with antibodies to γ-tubulin (Fig. 3 *B*, *panel 2*) or antibodies to cyclin B (Fig. 3 *B*, *panel 3*). Note that the cyclin B signal decreases from *M* to *T*, while the levels of pericentrin and γ-tubulin do not appear to change during this time. (*C*) Changes in lattice structure closely correlate with changes in the levels of centrosome-associated protein. The pericentrin lattice is simplest in G1 and enlarges to maximal size and complexity at G2, before separating to form a pair of centrosomes whose combined size at metaphase (*M*) is slightly larger than the G2 centrosome. When cells exit mitosis, the lattice rapidly returns to its simplest form (similar to that seen in G1). Similar results were observed with antibodies to γ-tubulin. Cell cycle stages: *G1*; *S*; *G2*; *M*, metaphase; *A*, anaphase; and *T*, telophase. Bar, 1 μm.

assemble at the centrosome to form the unique lattice structure (Fig. 10). Support for this idea comes from the tight correlation between protein accumulation at the centrosome and lattice growth (Fig. 8) and the ability to inhibit lattice growth by immunodepletion of pericentrin and γ-tubulin (Dictenberg, J., and S. Doxsey, unpublished observations). Pericentrin may play a direct role in the assembly process since it can induce the formation of ectopic centrosomes containing both pericentrin and γ-tubulin when overexpressed in cultured cells (Purohit, A., and S. Doxsey, manuscript in preparation). On the other hand, the γ-TuRC appears to lack assembly properties since purified fractions of the γ-TuRC are unable to assemble onto salt-stripped centrosomes (Moritz, M., Y. Zheng, and B. Alberts. 1996. *Mol. Biol. Cell.*, 7:207*a*). It is possible that the proteins assemble together as a large complex (Fig. 10) since they accumulate at the centrosome with indistinguishable kinetics (Fig. 8 *A*) and they remain in close proximity once assembled at the centrosome (Fig. 7). In addition, both appear to assemble together as tiny particles in living cells expressing GFP-pericentrin (Young, A., and S. Doxsey, unpublished observations). It is also possible that the proteins assemble (and disassemble) as separate subcomplexes and that assembly requires other proteins and factors.

The Pericentrin–γ-Tubulin Lattice as the Higher Order Organization of Microtubule Nucleating Sites at the Centrosome

The structure of the centrosome has remained an elusive biological problem for over a century. The use of an advanced algorithm for improved deconvolution of immunofluorescence images has provided a new view of this organelle. A major strength of this approach is the ability to uncover centrosome structure through the three-dimensional analysis of specific molecular components as shown here for pericentrin and γ-tubulin. Although the resolution is considerably less than that obtained by electron microscopy (70–100 nm), the method overcomes many of the problems associated with immunoelectron microscopic techniques such as reagent penetration and compromised antigenicity (Griffiths, 1993) and may thus provide a clearer representation of centrosome structure at these intermediate magnifications. This high resolution immunofluorescence imaging method, together with FRET analy-

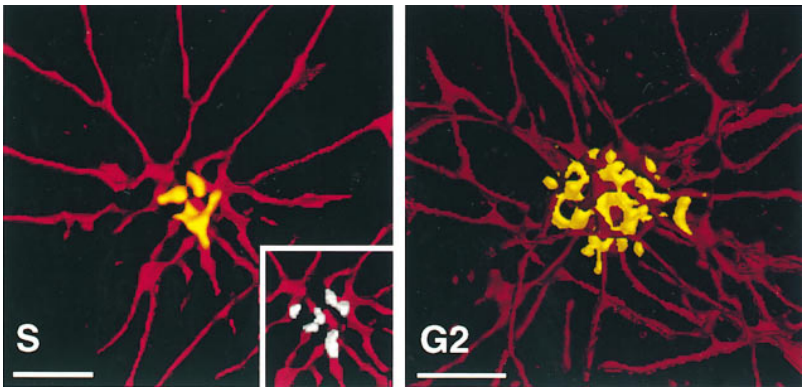

Figure 9. Nucleated microtubules contact the lattice. Images of nucleated microtubules (*red*) and pericentrin (*yellow*) have been merged to show that the number of nucleated microtubules converging at the centrosome (many bundled in *G2*) and the size of the pericentrin lattice increase from *S* to *G2* (also see Fig. 8, *A* and *C*). The inset in the first panel shows microtubule–lattice contacts in the simple early S phase centrosome. Inset shows the area of interaction (*white*) demonstrating near complete overlap of microtubule ends with lattice elements. See Materials and Methods. Similar results were obtained with γ-tubulin. Bars, 1 μm.

sis, will provide a powerful tool to study the organization and relationship of various molecular components at centrosomes, spindles, and other sites in the cell.

Although we have not determined the precise molecular arrangement of pericentrin and γ-tubulin within the lattice, it is possible that pericentrin forms the backbone of the structure tethering pericentrin–γ-tubulin complexes at the centrosome (Fig. 10). Pericentrin is predicted to be a large coiled-coil protein (Doxsey et al., 1994), which could serve as a molecular building block for the lattice in much the same way as coiled-coil intermediate filament proteins serve as subunits in the assembly of intermediate filaments (Albers and Fuchs, 1992). Other proteins most likely contribute to lattice organization, although we have not identified any that colocalize to the structure. The structural arrangement of other essential centrosome and mitotic spindle proteins (McNally et al., 1996; Walczak and Mitchison, 1996; Merdes and Cleveland, 1997) should provide information on the overall organization of centrosomes and spindles at a level unattainable by other methods.

Our results indicate that the lattice represents the organized arrangement of microtubule nucleating sites at the centrosome (Fig. 10). This idea is analogous to one proposed previously by Mazia (1987) that depicts the centrosome as a "string of microtubule initiating units" folded into a compact structure. In our model, the microtubule initiating units are pericentrin/γ-tubulin complexes linked together to form the lattice elements or "strings." The overall configuration of the lattice may account for the distinct microtubule arrangements observed in different MTOCs, such as the sharply focused arrays formed by compact centrosomes and the elongated, less-focused ar-

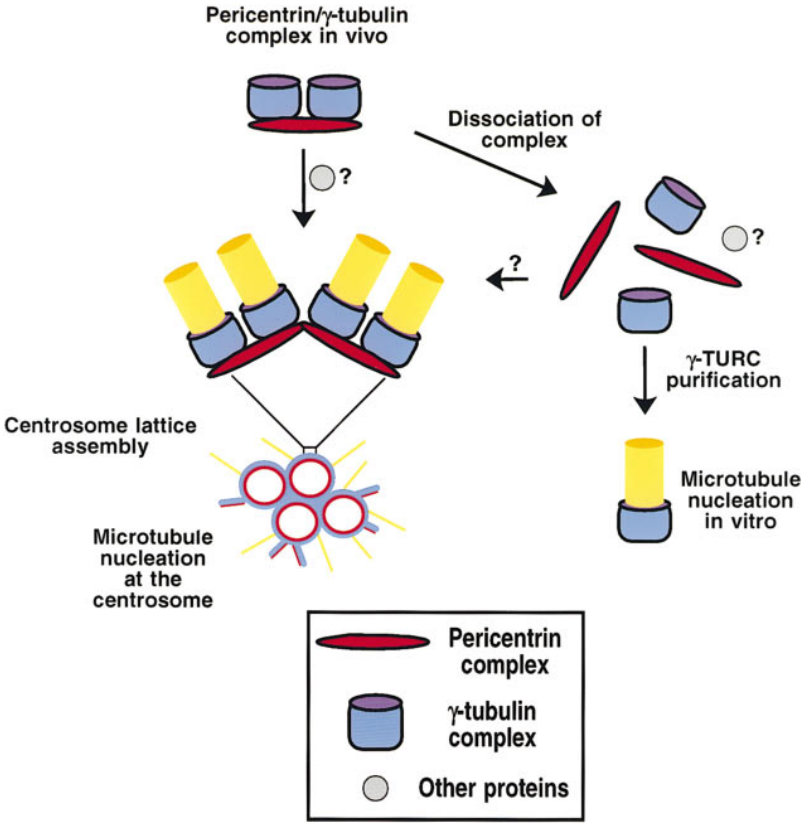

Figure 10. A model for centrosome assembly. The stoichiometry of pericentrin and γ-tubulin is consistent with a large complex consisting of one pericentrin complex and two γ-tubulin complexes. This model accommodates both of the current schemes proposed for microtubule nucleating complexes (Zheng et al., 1995; Erickson and Stoffler, 1996) (see Discussion). The complex appears to assemble at the centrosome to form a unique lattice (*left*). When dissociated, the complex gives rise to a pericentrin subcomplex, a γ-tubulin subcomplex and perhaps other proteins (*right*). Whereas the γ-tubulin subcomplex has not been characterized in this study, it has previously been shown that purified γ-TuRCs are capable of nucleating microtubules in vitro but are unable to assemble onto centrosomes (see Discussion). The pericentrin complex may facilitate assembly of γ-tubulin complexes into the centrosome lattice. Centrosome assembly and stabilization are likely to require other proteins.

rays that emanate from mouse meiotic spindle poles (Fig. 5, *C* and *D*). Within the lattice are regions that do not appear to nucleate microtubules, although both pericentrin and γ-tubulin are found there (Fig. 9, see microtubule-free regions in *yellow*). If these regions represent potential microtubule nucleation sites as we predict, the mechanism by which they acquire the ability to nucleate microtubules will be an important future area of investigation.

We dedicate this manuscript to the memory of Fredric S. Fay who served as an inspiration for this work and a spirited friend.

Special thanks to D. Mazia whose excitement and advice about centrosomes were invaluable during the course of this work. We also thank the following individuals for their assistance: D. Schmidt (UMMC) for FRET analysis; L. Boyer for gel filtration; R. Craig (UMMC) and colleagues for rapid freeze; J. Gosslin (UMMC) for mouse oocytes; J. Burkhardt (UCSF) for monoclonal antibody production; L. Lifschitz, K. Fogarty, and D. Bowman (UMMC) for image analysis; T. Stearns (Stanford University, Palo Alto, CA), P. Draber (Academy of Sciences of the Czech Republic), R. Vallee (Worcester Foundation, Shrewsbury, MA), J. Salisbury (Mayo Clinic, Rochester, MN) for antibodies, B. Oakley for γ-tubulin clones; and R. Tsein (University of California, San Diego, CA) for GFP constructs. For discussions and comments on the manuscript we thank M. Kirschner, R. King, R. Vallee, R. Davis, and A. Pereira.

S.J. Doxsey is a recipient of an Established Investigator Award from the American Heart Association (96-276). This work was supported by grants from the American Cancer Society (IRG-203) to S.J. Doxsey, from the National Institutes of Health (RO1GM51994 and RO1 RR09799-01A1) to S.J. Doxsey and W. Carrington, respectively, and from the National Science Foundation (BIR-9200027 and DBI-9724611) to F.S. Fay and W. Carrington, respectively.

Received for publication 25 November 1997 and in revised form 19 January 1998.

References

Adams, S.R., A.T. Harootunian, Y.J. Buechler, S.S. Taylor, and R.Y. Tsien. 1991. Fluorescence ratio imaging of cyclic AMP in single cells. *Nature.* 349: 694–697.

Albers, K., and E. Fuchs. 1992. The molecular biology of intermediate filaments. *Int. Rev. Cytol.* 134:243–279.

Archer, J., and F. Solomon. 1994. Deconstructing the microtubule-organizing center. *Cell.* 76:589–592.

Blomberg, M., and S.J. Doxsey. 1998. Rapid isolation of centrosomes. *Methods Enzymol.* In press.

Brown, R., S.J. Doxsey, L. Hong-Brown, R.L. Martin, and W. Welsh. 1996. Molecular chaperones and the centrosome: a role for TCP-1 in microtubule nucleation. *J. Biol. Chem.* 271:824–832.

Carrington, W., R.M. Lynch, E.D. Moore, G. Isenberg, K.E. Fogarty, and F.S. Fay. 1995. Superresolution three-dimensional images of fluorescence in cells with minimal light exposure. *Science.* 268:1483–1486.

DeDuve, C.J., J. Berthet, and H. Beaufay. 1959. Gradient centrifugation of cell particles: theory and applications. *Prog. Biphys. Biophys. Chem.* 236:1372–1379.

DeHaen, C. 1987. Molecular weight standards for calibration of gel filtration and sodium dodecyl sulfate-polyacrylamide electrophoresis: ferritin and apoferritin. *Anal. Biochem.* 166:235–245.

Doxsey, S.J., P. Stein, L. Evans, P. Calarco, and M. Kirschner. 1994. Pericentrin, a highly conserved protein of centrosomes involved in microtubule organization. *Cell.* 76:639–650.

Echeveri, C.J., B.M. Paschal, K.T. Vaughan, and R.B. Vallee. 1996. Molecular characterization of the 50-kD subunit of dynactin reveals function for the complex in chromosome alignment and spindle organization during mitosis. *J. Cell Biol.* 132:617–633.

Erickson, H.P., and D. Stoffler. 1996. Protofilaments and rings, two conformations of the tubulin family conserved from bacterial FtsZ to α/β and γ tubulin. *J. Cell Biol.* 135:5–8.

Felix, M.-A., C. Antony, M. Wright, and B. Maro. 1994. Centrosome assembly in vitro: Role of γ-tubulin recruitment in *Xenopus* sperm after formation. *J. Cell Biol.* 124:19–31.

Gard, D., S. Hafezi, T. Zhang, and S.J. Doxsey. 1990. Centrosome duplication continues in cycloheximide-treated *Xenopus* blastulae in the absence of a detectable cell cycle. *J. Cell Biol.* 110:2033–2042.

Gould, R.R., and G.G. Borisy. 1977. The pericentriolar material in Chinese hamster ovary cells nucleates microtubule formation. *J. Cell Biol.* 73:601–615.

Griffiths, G. 1993. Fine Structure Immunocytochemistry. Springer-Verlag, New York. 1–16.

Harlow, E., and D. Lane. 1988. Antibodies: A Laboratory Manual. Cold Spring Harbor Laboratory, Cold Spring Harbor, New York. 484–521.

Heim, R., A.B. Cubbit, and R. Tsien. 1995. Improved green fluorescence. *Nature.* 373:663–664.

Jacobson, M.P., P.R. Willis, and D.J. Winzor. 1996. Thermodynamic analysis of the effects of small inert cosolutes in the ultracentrifugation of noninteracting proteins. *Biochemistry.* 35:13173–13179.

Kellogg, D.R., M. Moritz, and B.M. Alberts. 1994. The centrosome and cellular organization. *Annu. Rev. Biochem.* 63:639–674.

Kuriyama, R., and G.G. Borisy. 1981. Microtubule-nucleating activity of centrosomes in chinese hamster ovary cells is independent of the centriole cycle but coupled to the mitotic cycle. *J. Cell Biol.* 91:822–826.

Lifschitz, L., E. Collins, J. Moore, and J. Gauch. 1994. Computer vision and graphics in fluorescence microscopy. *Proceedings of the Biomedical Imaging Workshop.* Institute of Electrical and Electronic Engineers. Computer Soc. Press, Los Angeles. 166–175.

Ludwig, M., N.F. Hensel, and R.J. Hartman. 1992. Calibration of a resonance energy transfer imaging system. *Biophys. J.* 61:845–857.

Martin, R.G., and B.N. Ames. 1960. A method for determining the sedimentation behavior of enzymes: application to protein mixtures. *J. Biol. Chem.* 236:1372–1379.

Mazia, D. 1987. The chromosome cycle and the centrosome cycle in the mitotic cycle. *Intl. Rev. Cytol.* 100:49–93.

McNally, F.J., K. Okawa, A. Iwamatsu, and R.D. Vale, 1996. Katanin, the microtubule-severing ATPase, is concentrated at centrosomes. *J. Cell Sci.* 109: 561–567.

Merdes, A., and D.W. Cleveland. 1997. Pathways of spindle pole formation: Different mechanisms; conserved components. *J. Cell Biol.* 138:953–956.

Miyawaki, A., J. Llopis, J.M. McCaffrey, J.A. Adams, M. Ikura, and R.Y. Tsien. 1997. Fluorescence indicators for calcium based on green fluorescent proteins and calmodulin. *Nature.* 388:882–887.

Mogensen, M, J., C. Mackie, S. Henderson, S.J. Doxsey, T. Stearns, and J. Tucker. 1997. Centrosomal deployment of gamma tubulin and pericentrin: evidence for a microtubule nucleating domain and a minus end docking domain in mouse epithelial cells. *Cell Motil. Cytoskeleton.* 36:276–290.

Moritz, M., M.B. Braunfeld, J.W. Sedat, B. Alberts, and D.A. Agard. 1995. Microtubule nucleation by γ-tubulin-containing rings in the centrosome. *Nature.* 378:638–640.

Murray, A.W., and M.W. Kirschner. 1989. Cyclin synthesis drives the early embryonic cell cycle. *Nature.* 339:275–280.

Nicolas, M.-T., and J-M. Bassot. 1993. Freeze substitution after fast-freeze fixation in preparation for immunocytochemistry. *Microsc. Res. Tech.* 24:474–487.

Novakova, M., E. Draberova, W. Schurmann, G. Czihak, V. Viklicky, and P. Draber. 1996. γ-tubulin redistribution in taxol-treated mitotic cells probed by monoclonal antibodies. *Cell Motil. Cytoskeleton.* 33:38–51.

Oakley, C.E., and B.R. Oakley. 1989. Identification of gamma tubulin, a new member of the tubulin superfamily encoded by mipA gene of *Aspergillus nidulans*. *Nature.* 338:662–664.

Prasher, D.C., V.D. Eckenrode, W.W. Ward, F.G. Prendergast, and M.J. Cormier. 1992. Primary structure of the Aequorea victoria green-fluorescent protein. *Gene.* 111:229–233.

Salisbury, J.L. 1995. Centrin, centrosomes and mitotic spindle poles. *Curr. Opin. Cell Biol.* 7:39–45.

Sawin, K.E., and T.J. Mitchison. 1991. Poleward microtubule flux in mitotic spindles assembled in vitro. *J. Cell Biol.* 112:941–954.

Siegel, L.M., and K.J. Monty. 1966. Determination of molecular weights and frictional ratios of proteins in impure systems by use of gel filtration and density gradient centrifugation: application to crude preparations of sulfite and hydroxylamine reductases. *Biochem. Biophys. Acta.* 112:346–362.

Sparks, C., E. Fey, C. Vidair, and S.J. Doxsey. 1995. Phosphorylation of NuMA occurs during nuclear breakdown not spindle assembly. *J. Cell Sci.* 108:3389–3396.

Stearns, T., and M. Kirschner. 1994. Reconstitution of centrosome assembly, role of γ tubulin. *Cell.* 76:623–637.

Stryer, L. 1978. Fluorescence energy transfer as a spectroscopic ruler. *Annu. Rev. Biochem.* 47:819–846.

Urata, Y., S.J. Parmalee, D.A. Agard, and J.W. Sedat. 1995. A three-dimensional structural dissection of Drosophila polytene chromosomes. *J. Cell Biol.* 131:279–295.

Vogel, J.M., T. Stearns, C.L. Rieder, and R.E. Palazzo. 1997. Centrosomes isolated from *Spisula solidissima* oocytes contain rings and an unusual stoichiometric ratio of α/β tubulin. *J. Cell Biol.* 137:193–202.

Walczak, C.E., and T.J. Mitchison. 1996. Kinesin-related proteins at mitotic spindle poles: function and regulation. *Cell.* 85:943–946.

Wilson, E.B. 1925. The Cell in Development and Heredity. Third Edition. Macmillan, Inc., New York. 1–7.

Wu, P., and L. Brand. 1994. Resonance energy transfer: Methods and applications. *Anal. Biochem.* 218:1–13.

Young, A., R.A. Tuft, W. Carrington, and S.J. Doxsey. 1998. Centrosome dynamics in living cells. *Methods Cell Biol.* In press.

Zheng, Y., M.L. Wong, B. Alberts, and T. Mitchison. 1995. Nucleation of microtubule assembly by a γ tubulin-containing ring complex. *Nature.* 378:578–583.